



Short communication

Double-diffusive natural convection in a rectangular cavity with partially thermally active side walls

Rasoul Nikbakhti, Asghar B. Rahimi*

Faculty of Engineering, Ferdowsi University of Mashhad, P.O. Box No. 91775-1111, Mashhad, Iran

ARTICLE INFO

Article history:

Received 17 June 2011

Received in revised form 4 February 2012

Accepted 10 February 2012

Available online 16 March 2012

Keywords:

Double diffusive convection

Partially active walls

Aspect ratios

Rectangular cavity

Heat and mass transfer

ABSTRACT

Double-diffusive natural convection in a rectangular cavity with partially thermally active side walls filled with air is studied numerically. The active part of the left side wall has a higher temperature and concentration than the right side one. The length of the thermally active part is equal to half of the cavity height. The top and bottom of the cavity and inactive part of the side walls are considered to be adiabatic and impermeable to mass transfer. Placement order of thermal active walls has significant effect on heat and mass transfer rate, to explore this effect and achieving the optimum rate inside the cavity, nine different relative positions of the active zones are considered. The non-dimensional forms of governing transport equations describing double-diffusive natural convection for laminar two-dimensional incompressible flow are functions of vorticity, temperature or energy, concentration and stream-function. Laminar regime is considered under steady state condition. The coupled differential equations are discretized by the finite difference method and are solved using the successive-over-relaxation (SOR) method. The results are obtained for different heating sections and different parameters such as aspect ratio, buoyancy ratio and Schmidt number. Also the heat and mass transfer rate in the cavity is measured in terms of the average Nusselt and Sherwood numbers.

© 2012 Taiwan Institute of Chemical Engineers. Published by Elsevier B.V. All rights reserved.

1. Introduction

During the past 50 years many experimental and numerical studies have been carried out concerning convective phenomena within cells. Most of these studies deal with fluid motion due to temperature gradients only. Nevertheless, fluid motion may be induced by density variations due to gradients of other scalar quantities. One of these quantities can be pollutant concentration within the fluid. Such a phenomenon combining temperature and concentration buoyancy forces is called double-diffusion. Double-diffusion occurs in a very wide range of fields such as oceanography, astrophysics, geology, biology, and chemical processes, as well as in many engineering applications such as solar ponds, natural gas storage tanks, crystal manufacturing, and metal solidification processes. Unique double diffusive convection phenomena, such as salt fingers and diffusive interfaces have been observed due to the significant differences in diffusivities of heat and mass [1]. There are many convection modes depending on the directions of temperature and concentration gradients relative to gravity, as pointed out by Ostrach [2]. Gebhart and Pera [3] were among the first ones to numerically study double-diffusion for cases of

vertical laminar fluid motions along surfaces or in plumes. In their study, special attention was paid to the influence of non-dimensional parameters relevant to double-diffusion and on the heat and mass transport processes transition to turbulence was mentioned. In 1985, Bejan [4] completed a fundamental study of scale analysis relative to heat and mass transport processes within cavities. Pure thermal convection, pure solutal convection, heat transfer driven flows, and mass transfer driven flows were taken into account. Nishimura *et al.* [5] studied numerically the oscillatory double-diffusive convection in a rectangular enclosure with combined horizontal temperature and concentration gradients. They concluded that the oscillatory double-diffusive convection with the secondary cell flow structure occurs for a certain range of buoyancy ratio from $N = 1.044$ to 1.122 . Chamkha and Al-Naser [6,7] studied numerically the hydro magnetic double diffusive convection in a rectangular enclosure. Their cavity and conditions were similar to that of Nishimura [5] but they imposed magnetic field and heat generation. Costa [8,9] numerically studied the double-diffusive natural convection in different enclosure geometries such as square and parallelogram. Papanicolaou and Belessiotis [10] numerically studied the double-diffusive natural convection in an asymmetric trapezoidal enclosure with vertical temperature and concentration gradients. Al-Amiri *et al.* [11] investigated steady mixed convection in a square lid-driven cavity under the combined buoyancy effects of thermal and mass

* Corresponding author.

E-mail address: rahimiab@yahoo.com (A.B. Rahimi).

Nomenclature

Ar	aspect ratio (H/L)
C	dimensional concentration (kg/m ³)
D	mass diffusivity (m ² /s)
g	acceleration of gravity (m/s ²)
Gr _S	solubility Grashof number, Gr _S = (gβ _S ∇ CL ³ /ν ²)
Gr _T	thermal Grashof number, Gr _T = (gβ _T ∇ TL ³ /ν ²)
H	height of the cavity (m)
L	length of the cavity (m)
Le	Lewis number, Le = (α/D) = (Sc/Pr)
M	center of the heating section (m)
N	buoyancy ratio, N = ((β _S (C _h - C _l))/(β _T (T _h - T _c)))
Nu	local Nusselt number
\overline{Nu}	average Nusselt number
P	pressure (kg/m s ²)
Pr	Prandtl number, Pr = ν/α
Sc	Schmidt number, Sc = ν/D
Sh	local Sherwood number
\overline{Sh}	average Sherwood number
T	temperature (K)
u, v	velocity components (m/s)
U, V	dimensionless velocity components
x, y	dimensional coordinates (m)
X, Y	dimensionless coordinates

Greek symbols

α	thermal diffusivity (m ² /s)
β _S	coefficient of solubility expansion (m ³ /kg)
β _T	coefficient of thermal expansion (K ⁻²)
ν	kinematic viscosity (m ² /s)
θ	dimensionless temperature
ρ	density (kg/m ³)
ω	vorticity (s ⁻¹)
ζ	dimensionless vorticity
ψ	stream function (m ² /s)
Ψ	dimensionless stream function

Subscripts

c	cold wall
h	hot wall and high concentration
l	low concentration

diffusion. Teamah [12] studied numerically double-diffusive convective flow in a rectangular enclosure with the upper and lower surfaces being insulated and impermeable. Constant temperatures and concentration are imposed along the left and right walls of the enclosure. In addition, a uniform magnetic field is applied in a horizontal direction. Chouikh *et al.* [13] studied numerically the natural convection flow resulting from the combined buoyancy effects of thermal and mass diffusion in an inclined cavity with differentially heated side walls. The double-diffusive convection recently has been studied [14–18] in different geometries and boundary conditions.

The present study deals with the double-diffusive natural convection in an enclosure filled with air and partially heated vertical walls for nine different combinations of heating section. That is, for the hot section placed at the top, middle and bottom and the same applies for the cold section. The task here is to determine in which combinations we have the maximum/minimum heat and mass transfer rate. The results are displayed graphically in terms of

the streamlines, isotherms and iso-concentration, which show the effect of the aspect ratio and buoyancy ratio with different heating sections of the side walls.

2. Mathematical formulation

A schematic diagram of the two-dimensional natural convection flow in a rectangular cavity of length L and height H filled with moist air with Pr = 0.71 and with concentration c_i , is shown in Fig. 1. The partially thermally active side walls of the cavity are maintained at two different but uniform temperatures and concentration, namely, $T_h, T_c (T_h > T_c)$ and $c_h, c_l (c_h > c_l)$, respectively. The inactive parts of the side walls and horizontal walls $y=0$ and $y=H$ are thermally insulated. The heat and mass transfer characteristics are investigated for nine different combinations of the heated active wall. That is, for the hot section located at the top, middle and bottom and the cold section moved from bottom to top. The length of the thermally active part is $h = H/2$. Placement order of thermal active section has significant effect on heat and mass transfer rate, to explore this effect and achieving the optimum rate inside the cavity, the following method is considered (state of the art). The fluid is assumed to be incompressible, Newtonian, and viscous. The viscous dissipation is assumed to be negligible. The heat flux driven by concentration gradients (thermal diffusion or Soret effect) and the mass flux driven by temperature gradients (diffusion thermo or Dufour effect) are neglected. The Boussinesq approximation with opposite thermal and solute buoyancy forces is used for the body force terms in the momentum equations. The governing equations for the problem under consideration are based on the balance laws of mass, momentum, energy, and concentration in two dimensions. Representing the position through Cartesian coordinate system and Taking into account the assumptions mentioned above, these equations can be written in dimensional form as the following:

$$\frac{\partial u}{\partial x} + \frac{\partial v}{\partial y} = 0 \quad (1)$$

$$u \frac{\partial u}{\partial x} + v \frac{\partial u}{\partial y} = -\frac{1}{\rho_0} \frac{\partial P}{\partial x} + \nu \left[\frac{\partial^2 u}{\partial x^2} + \frac{\partial^2 u}{\partial y^2} \right] \quad (2)$$

$$u \frac{\partial v}{\partial x} + v \frac{\partial v}{\partial y} = -\frac{1}{\rho_0} \frac{\partial P}{\partial y} + \nu \left[\frac{\partial^2 v}{\partial x^2} + \frac{\partial^2 v}{\partial y^2} \right] - \frac{\rho}{\rho_0} \quad (3)$$

$$u \frac{\partial T}{\partial x} + v \frac{\partial T}{\partial y} = \alpha \left[\frac{\partial^2 T}{\partial x^2} + \frac{\partial^2 T}{\partial y^2} \right] \quad (4)$$

$$u \frac{\partial c}{\partial x} + v \frac{\partial c}{\partial y} = D \left[\frac{\partial^2 c}{\partial x^2} + \frac{\partial^2 c}{\partial y^2} \right] \quad (5)$$

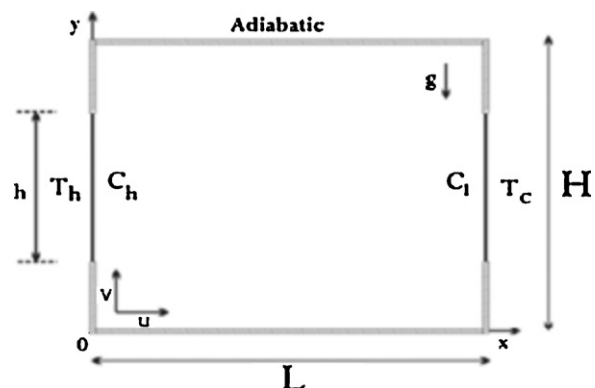


Fig. 1. Physical configuration.

The mixture density is assumed to be uniform over all the cavity, exception made to the buoyancy term, in which it is taken as a function of both the temperature and concentration levels through the Boussinesq approach

$$\rho = \rho_0[1 - \beta_T(T - T_c) + \beta_S(c - c_1)] \quad (6)$$

The appropriate boundary conditions are

$$u = v = 0, T = T_c, C = C_1, \quad x = 0, m - \frac{h}{2} \leq y \leq m + \frac{h}{2}, \quad u = v = 0, T = T_c, C = C_1,$$

$$x = L, m - \frac{h}{2} \leq y \leq m + \frac{h}{2}, \quad u = v = 0, \frac{\partial T}{\partial x} = 0, \frac{\partial C}{\partial x} = 0, \quad x = 0, L,$$

$$0 \leq y \leq m - \frac{h}{2}, m + \frac{h}{2} \leq y \leq H, \quad u = v = 0, \frac{\partial T}{\partial y} = 0, \frac{\partial C}{\partial y} = 0, \quad y = 0, H.$$

Introducing the following non-dimensional variables

$$X = \frac{x}{L}, \quad Y = \frac{y}{H}, \quad M = \frac{m}{H}, \quad U = \frac{uL}{\nu}, \quad V = \nu \frac{L^2}{\nu H}, \quad \Psi = \frac{\psi L}{\nu H}, \quad \zeta = \frac{\omega HL}{\nu}, \quad \theta = \frac{(T - T_c)}{(T_h - T_c)}, \quad C = \frac{(c - c_1)}{(c_h - c_1)}$$

We get the vorticity-stream function formulation of the above problems (1)–(5) as

$$U \frac{\partial \zeta}{\partial X} + V \frac{\partial \zeta}{\partial Y} = \frac{\partial^2 \zeta}{\partial X^2} + \frac{1}{Ar^2} \frac{\partial^2 \zeta}{\partial Y^2} + ArGr_T \frac{\partial \theta}{\partial X} - ArGr_S \frac{\partial C}{\partial X} \quad (7)$$

$$U \frac{\partial \theta}{\partial X} + V \frac{\partial \theta}{\partial Y} = \frac{1}{Pr} \left[\frac{\partial^2 \theta}{\partial X^2} + \frac{1}{Ar^2} \frac{\partial^2 \theta}{\partial Y^2} \right] \quad (8)$$

$$U \frac{\partial C}{\partial X} + V \frac{\partial C}{\partial Y} = \frac{1}{Sc} \left[\frac{\partial^2 C}{\partial X^2} + \frac{1}{Ar^2} \frac{\partial^2 C}{\partial Y^2} \right] \quad (9)$$

where

$$-\zeta = Ar^2 \frac{\partial^2 \Psi}{\partial X^2} + \frac{\partial^2 \Psi}{\partial Y^2} \quad (10)$$

The non-dimensional parameters that appear in the equations are: Pr the Prandtl number, Gr_T the thermal Grashof number, Gr_S the solutal Grashof number and Sc the Schmidt number. Parameter $N = ((\beta_S(c_h - c_1))/(\beta_T(T_h - T_c)))$ is the buoyancy ratio, which is the ratio between the solute and thermal buoyancy forces. It can be either positive or negative and its sign depends on the coefficients β_T and β_S . In this paper positive sign is used for buoyancy ratio. According to the section of the pollutant concentration on the hot or cold vertical walls, the solutal and thermal buoyancy forces may be either augmenting or opposing each other. So depending on the directions of the buoyancy forces, the problem can be either an aiding or opposing buoyancy condition. The local Nusselt number and Sherwood number is defined by $Nu = (-\partial\theta/\partial X)_{X=0}$, $Sh = (-\partial C/\partial X)_{X=0}$ resulting in the average Nusselt number and Sherwood number as $\bar{Nu} = (1/h) \int_h Nu dY$, $\bar{Sh} = (1/h) \int_h Sh dY$ and $h = H/2$ is height of heating section. The boundary conditions in the dimensionless form are

$$\Psi = \frac{\partial \Psi}{\partial Y} = 0, \theta = 1, C = 1, \quad X = 0, M - \frac{1}{2} \leq Y \leq M + \frac{1}{2}, \quad \Psi = \frac{\partial \Psi}{\partial Y} = 0, \theta = 0, C = 0,$$

$$X = 1, M - \frac{1}{2} \leq Y \leq M + \frac{1}{2}, \quad \Psi = 0, \frac{\partial \theta}{\partial X} = 0, \frac{\partial C}{\partial X} = 0, \quad \text{at } X = 0 \text{ and } 1$$

$$0 \leq Y \leq M - \frac{1}{2}, M + \frac{1}{2} \leq Y \leq 1, \quad \Psi = \frac{\partial \Psi}{\partial Y} = 0, \frac{\partial \theta}{\partial Y} = 0, \frac{\partial C}{\partial Y} = 0, \quad \text{at } Y = 0 \text{ and } 1.$$

3. Method of solution

The governing equations along with the boundary conditions are solved numerically, employing finite-difference techniques. The region of interest was covered with 'm' vertical and 'n' horizontal uniformly spaced grid lines. The vorticity transport, energy and mass equations are solved using the ADI (Alternating Direction Implicit) method and the stream function equation is solved by SOR (successive over-relaxation) method. The over-relaxation parameter is chosen to be 1.8 for stream function solutions. The buoyancy and diffusive terms are discretized by using central differencing while the use of upwind differencing is preferred for convective terms for numerical stability. Starting from arbitrarily specified initial values of variables, the discretized transient equations are then solved by marching in time until an asymptotic steady-state solution is reached. Convergence of iteration for stream function solution is obtained at each time step. The following criterion is employed to check for steady-state solution

$$\frac{\sum \sum |\Phi_{i,j}^{k+1} - \Phi_{i,j}^k|}{|\Phi|_{\max} \times m \times n} \leq \varepsilon \quad (11)$$

where Φ stands for Ψ , ζ or θ ; k refers to time and i and j refer to space coordinates. The value of ε is chosen as 10^{-5} . The time step used in the computations is varied between 0.00001 and 0.004 depending on Grashof number and mesh size. The numerical solutions are found for different grid systems from 21×21 to 101×101 for $Ar = 1$ and it is observed that a further refinement of grids from 51×51 to 101×101 does not have a significant effect on the results in terms of average Nusselt and Sherwood number and the maximum value of the stream function. Based on this observation, a uniform grid of 51×51 points is used for all of the calculations for $Ar = 1$. Similar grid dependency studies carried out for the other aspect ratios and an optimum grid size is obtained for each aspect ratio.

4. Results and discussion

In this paper, the results are presented in the form of streamlines, isotherms and iso-concentrations for different heating sections to show the fluid flow, heat and mass transfer phenomena in steady states. The rate of heat and mass transfer in the enclosure is measured in terms of the average Nusselt number and average Sherwood number. The flow patterns, isotherms and iso-concentrations for different heating sections, $Ar = 2$ and $Gr_T = 10^6$, $Sc = 2$ and $N = 0.2$ are displayed in Figs. 2, 3 and 4(a)–(i). The flow is unicellular with clockwise rotation. In Fig. 2(a), both of heating sections have been placed on the upper sidewall of the cavity. Fig. 2(i) is mirror image of Fig. 2(a), which both of heating sections have been placed on the lower sidewall of the cavity. When heating sections are top-middle or middle-bottom, two secondary cells have been inserted in principal cell located near thermally active parts of the sidewalls, while the remaining parts of the cavity remains intact. In the top-bottom active section, something strange happens. It is observed in Fig. 2(c) that the current is in both cells and the center of cells place in the near part to the active sidewalls. In comparison to the other sections, velocity and circulation rate of this section is a minimum. In the middle-top, very small eddies are placed into the principal cell, which occupies nearly the entire cavity. Active section of bottom-

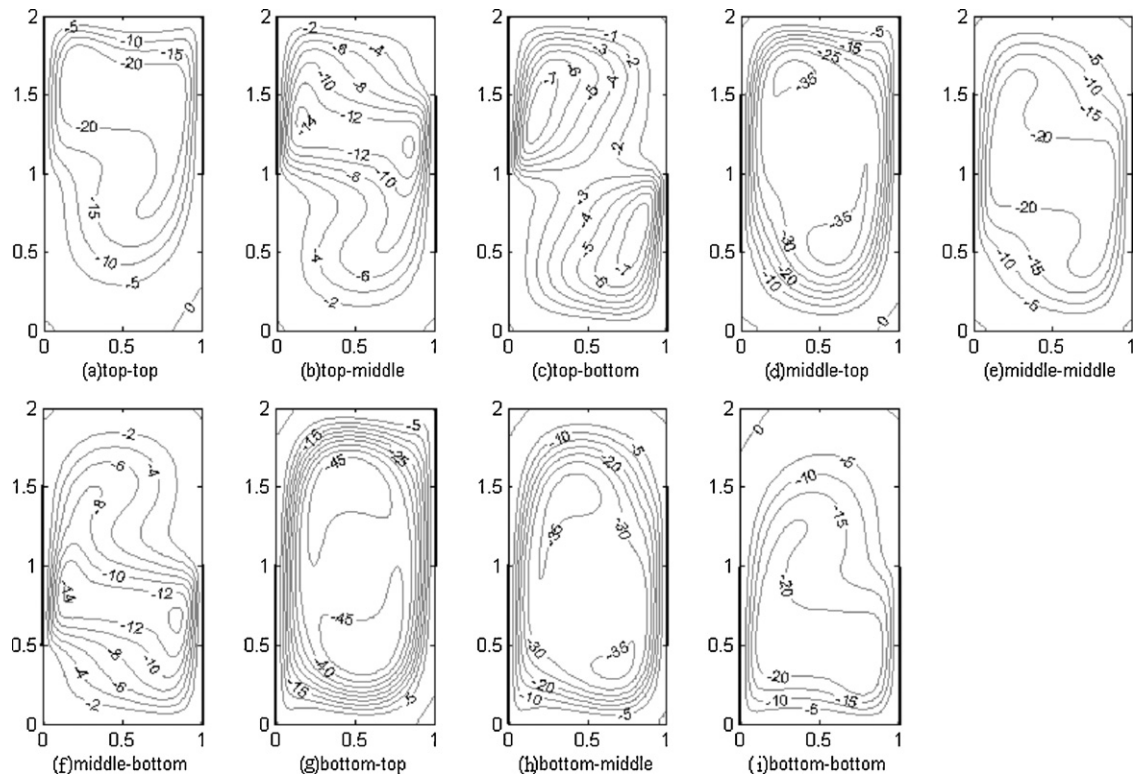


Fig. 2. Streamlines for all heating location, $Ar = 2$, $N = 0.2$, $Sc = 2$ and $Gr_T = 10^6$.

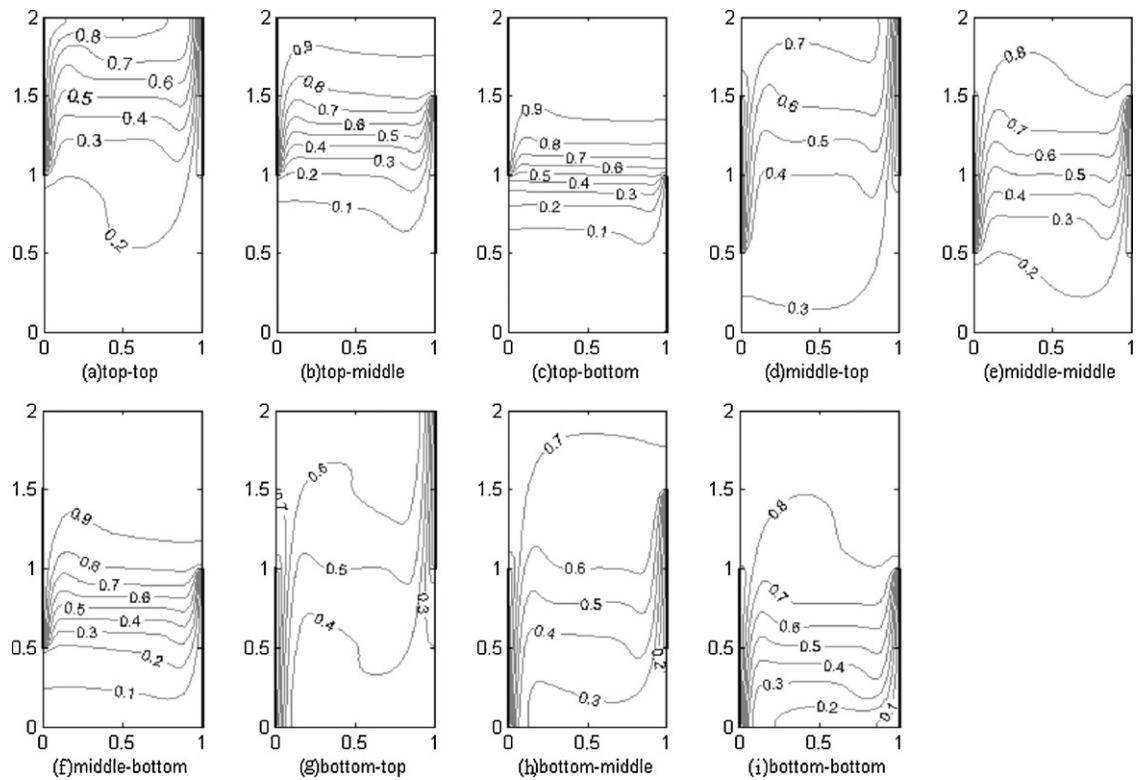


Fig. 3. Isotherms for all heating location, $Ar = 2$, $N = 0.2$, $Sc = 2$ and $Gr_T = 10^6$.

middle (Fig. 2(h)) is mirror image of active section of middle–top (Fig. 2(d)). In the bottom–top active section, clockwise principle cell occupies the entire cavity. Velocity and circulation rate in this case is a maximum (Fig. 2(g)). Fig. 3(a), illustrates isotherms in the

top region of cavity where active points are placed. When the cold active wall moves from top to bottom, Fig. 3(b) illustrates changes in which isotherms are located in the central part of the cavity and convection near to active sections are converted to conduction.

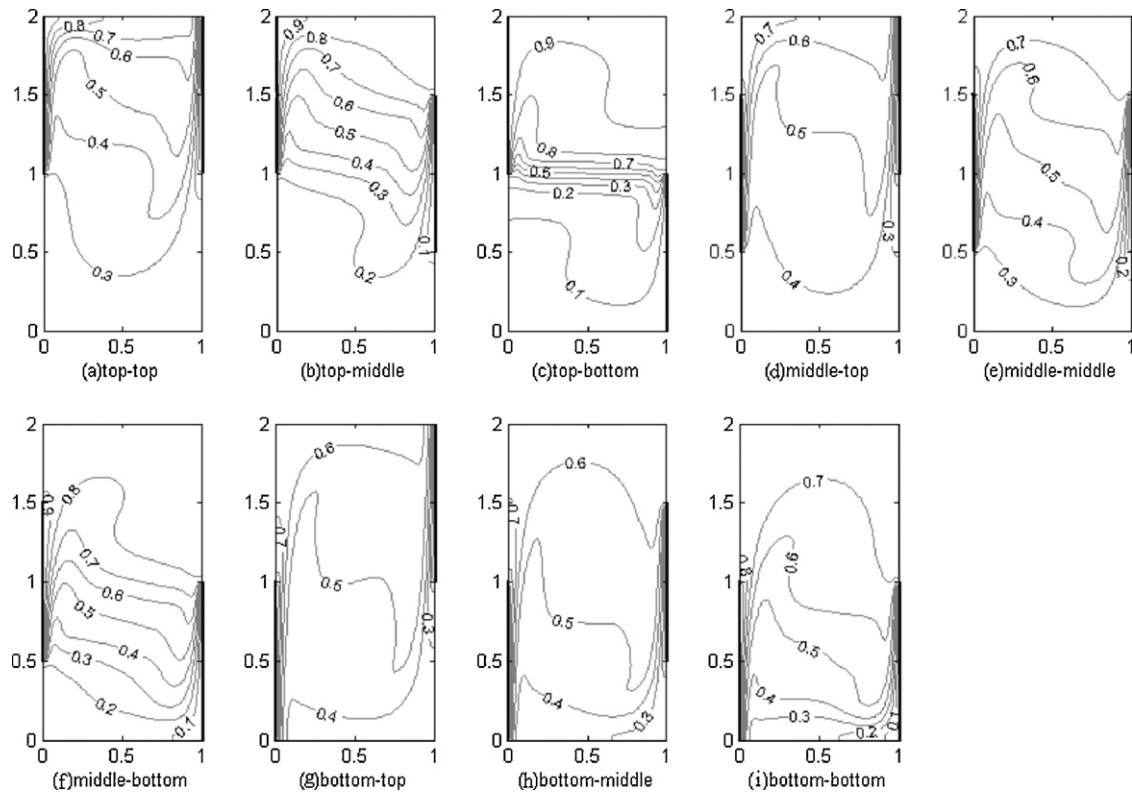


Fig. 4. Iso-concentrations for all heating location, $Ar = 2$, $N = 0.2$, $Sc = 2$ and $Gr_T = 10^6$.

With moving the cooling section toward lower part (Fig. 3(c)), isotherms predict conduction in the middle of the cavity. In this case, heat transfer rate in comparison to the other cases is very low. Fig. 3(i) and (f) is illustration of mirror images of Fig. 3(a) and (b), respectively. In middle–top and bottom–middle active sections, a

thermal boundary layer forms on the top and bottom part of cooling and heating sections, respectively, and convection is seen from isotherms of Fig. 3(h) and (d). Fig. 3(e) illustrates convection near the active sidewalls. In bottom–top active section, strong thermal boundary layers in the top part of cooling wall and bottom

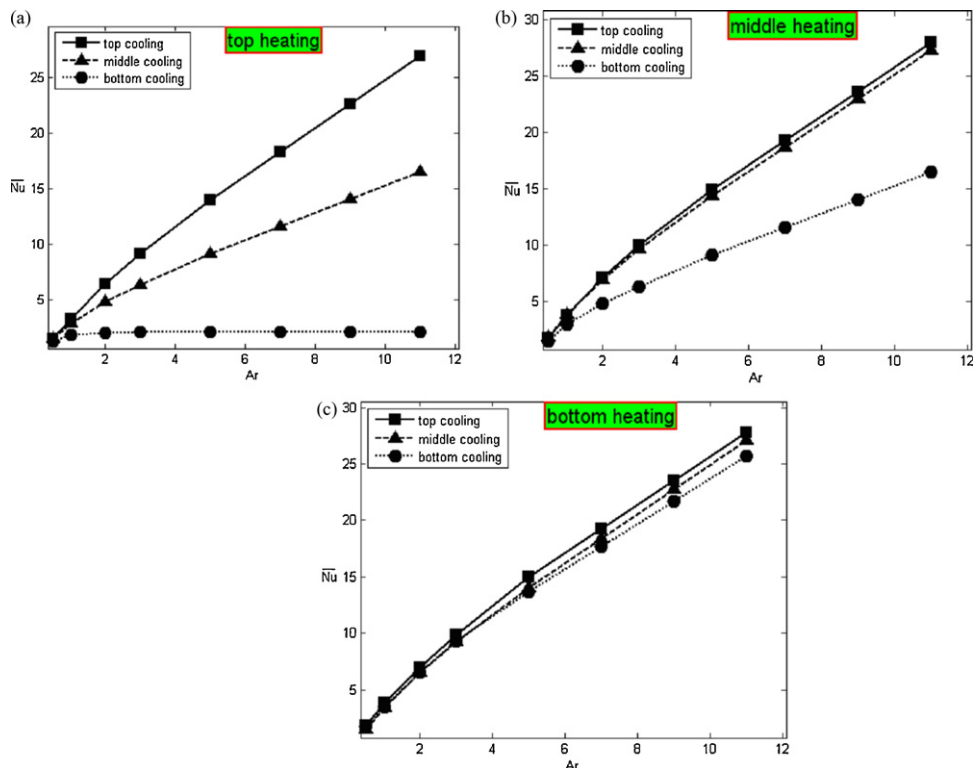


Fig. 5. Average Nusselt number for different heating location.

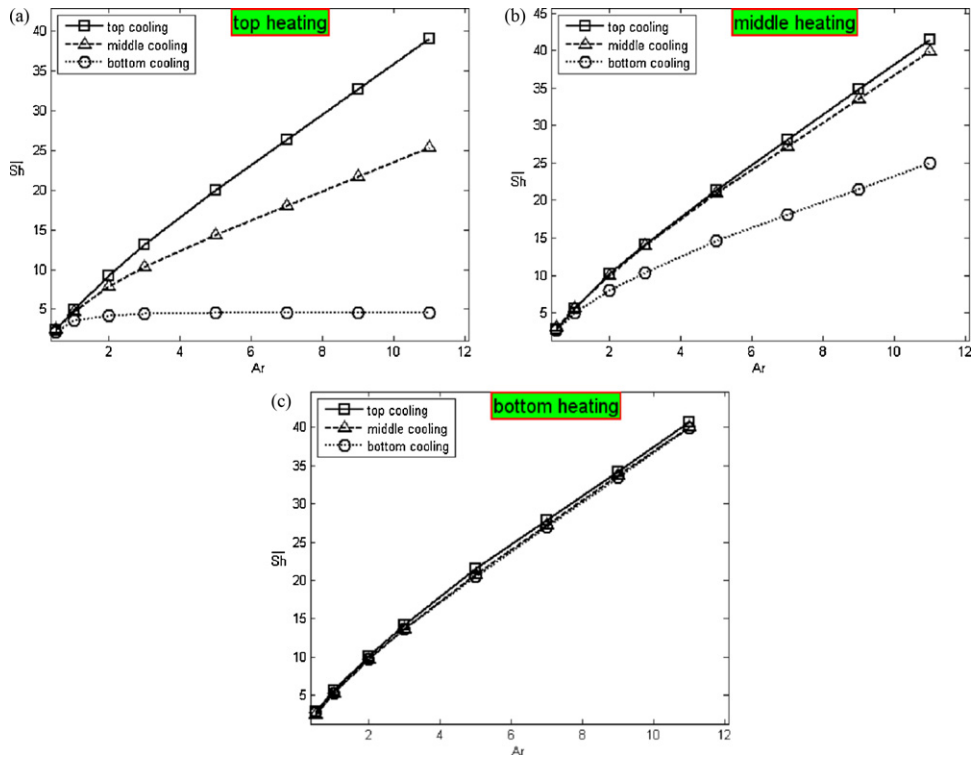


Fig. 6. Average Sherwood number for different heating location.

part of heating wall are formed shown in Fig. 3(g). In these cases, heat transfer rate, in comparison to all cases is a maximum. Fig. 4(a)–(i) depicts the isopleths of concentration. As it can be seen, the isopleths of concentration has the same behavior as the isopleths of temperature and this is, because of the similarity of energy equation and mass transfer equation. According to Schmidt number which is greater than Prandtl number, the thermal diffusivity has greater effect on fluid than the mass diffusivity does. So, formed solutal boundary layer in Fig. 4(d) and (h), compared with formed thermal boundary layer in Fig. 3(d) and (h) is thinner. Fig. 4(i) and (f) seems to be the mirror images of Fig. 4(a) and (b), respectively. In Fig. 4(e), the middle–middle active section exhibits convection near the active sections. Strong solutal boundary layers are formed at the active sections, as seen in Fig. 4(g). The circulation rate and the mass transfer rate are a maximum in this case compared to all the other cases. In order to assess how aspect ratio and different heating sections affect the heat and mass transfer, the average Nusselt and Sherwood number have been depicted in Figs. 5 and 6(a)–(c) as a function of aspect ratio for different heating sections. It is clear that, the heat and mass transfer rate is increased with increasing the aspect ratio. For $Ar \leq 1$, when heating sections change, there is not any dramatic change in the average Nusselt and Sherwood numbers. But, some changes in heating sections, the average Nusselt and Sherwood numbers are seen when aspect ratio is increased. From Figs. 5 and 6(a), it is noted that for fixed heating section on the top part of cavity and cooling section in the bottom the aspect ratio will not affect the average Nusselt and Sherwood numbers. From Figs. 5 and 6(c), it is seen that when heating section on the bottom part of cavity is fixed, cooling section does not cause considerable changes in heat and mass transfer rate and the heat and mass transfer rate is maximum in the cavity. With changing cooling section from bottom to top, the average Nusselt and Sherwood number increases with increase of aspect ratio. This can be observed in Figs. 5 and 6, respectively. Fig. 7 illustrates the influence of the buoyancy ratio N on the average Nusselt number in aiding and

opposing flows. It is observed that, in aiding flow the average Nusselt number is increased as the buoyancy ratio is increased. The increasing average Nusselt number in aiding flow is due to same direction of the solutal and thermal buoyancy forces. As a result, it is clear for $N \geq 1$ that the average Nusselt number is increased. The increasing average Nusselt number in aiding flow is representative of same direction effects of solutal buoyancy force and thermal buoyancy force in natural convection that causes increase of the heat transfer in the cavity. We notice that in opposing flow for $0 \leq N \leq 1$, the average Nusselt number is decreased as the buoyancy ratio is increased. After $N=0$ in an opposing flow due to transmission interchangeable effect from thermal and solutal buoyancy forces will be reduced with increasing buoyancy ratio average Nusselt number, where as in a critical point solutal and thermal buoyancy effects neutralize each other. In this point, buoyant convection flow is hindered and approximately $Nu = 1$.

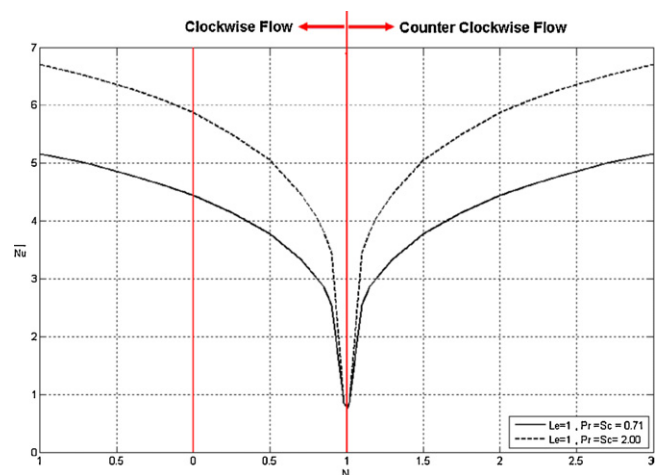


Fig. 7. Average Nusselt number versus buoyancy ratio in C.W. and C.C.W. flow.

Meanwhile, heat transmission is performed as conduction. The flows considered in this part are aiding or opposing flows, with $Le = 1$. Therefore average Nusselt number profile to the critical point $N = 1$ in opposing flow will be symmetrical. Fig. 7 illustrates the influence of the buoyancy ratio N on the average Nusselt number for various values of Schmit and Prandtl numbers. It can be noticed that with increasing Schmit number, the effects of mass transmission derived from increase in solutal buoyancy force on heat transmission increase and accordingly cause to increase the average Nusselt number in double diffusive natural convection.

5. Conclusions

A numerical model has been employed to analyze the flow, heat and mass transfer of air filled in a rectangular cavity with partially thermally active side walls. It is observed that the rate heat and mass transfer is high for the bottom–top thermally active section while the rate of heat and mass transfer is poor in the top–bottom thermally active section. The heat and mass transfer rate are found to increase with increase in the aspect ratio. It is found that in aiding flow, the average Nusselt number increase by increasing the buoyancy ratio. Thus the heat transfer rate is increased in the cavity. In opposing flow, with increase in buoyancy ratio till $N = 1$, the average Nusselt number is decreased. After critical point ($N = 1$) the rotating flow orientation change and with increase in buoyancy ratio, the average Nusselt number increase, so the heat transfer rate in the cavity is increased.

References

- [1] Turner JS. Buoyancy effects in fluids. London: Cambridge University Press; 1979.
- [2] Ostrach S. Fluid mechanics in crystal growth – the 1982 Freeman Scholar Lecture. *J Fluids Eng* 1983;105:5–20.
- [3] Gebhart B, Pera L. The nature of vertical natural convection flows resulting from the combined buoyancy effects of thermal and mass diffusion. *Int J Heat Mass Transfer* 1971;14:2025–50.
- [4] Bejan A. Mass and heat transfer by natural convection in a vertical cavity. *Int J Heat Fluid Flow* 1985;6:149–59.
- [5] Nishimura T, Wakamatsu M, Morega AM. Oscillatory double-diffusive convection in a rectangular enclosure with combined horizontal temperature and concentration gradients. *Int J Heat Mass Transfer* 1998;41:1601–11.
- [6] Chamkha AJ, Al-Naser H. Hydromagnetic double-diffusive convection in a rectangular enclosure with opposing temperature and concentration gradients. *Int J Heat Mass Transfer* 2002;45:2465–83.
- [7] Chamkha AJ, Al-Naser H. Hydromagnetic double-diffusive convection in a rectangular enclosure with uniform side heat and mass fluxes and opposing temperature and concentration gradients. *Int J Therm Sci* 2002;41:936–48.
- [8] Costa VAF. Double diffusive natural convection in a square enclosure with heat and mass diffusive walls. *Int J Heat Mass Transfer* 1997;40:4061–71.
- [9] Costa VAF. Double-diffusive natural convection in parallelogrammic enclosures. *Int J Heat Mass Transfer* 2004;47:2913–26.
- [10] Papanicolaou E, Belessiotis V. Double-diffusive natural convection in an asymmetric trapezoidal enclosure: unsteady behavior in the laminar and the turbulent-flow regime. *Int J Heat Mass Transfer* 2005;48:191–209.
- [11] Al-Amiri AM, Khanafer KM, Pop I. Numerical simulation of combined thermal and mass transport in a square lid-driven cavity. *Int J Therm Sci* 2007;46:662–71.
- [12] Teamah MA. Numerical simulation of double diffusive natural convection in rectangular enclosure in the presences of magnetic field and heat source. *Int J Therm Sci* 2008;47:237–48.
- [13] Chouikh R, Ben Snoussi L, Guizani A. Numerical study of the heat and mass transfer in inclined glazing cavity: application to a solar distillation cell. *Renew Energy* 2007;32:1511–24.
- [14] Nithyadevi N, Yang R-J. Double diffusive natural convection in a partially heated enclosure with Soret and Dufour effects. *Int J Heat Fluid Flow* 2009;30:902–10.
- [15] Teamah MA, El-Maghlany WM. Numerical simulation of double-diffusive mixed convective flow in rectangular enclosure with insulated moving lid. *Int J Therm Sci* 2010;49:1625–38.
- [16] Sheremet MA. The influence of cross effects on the characteristics of heat and mass transfer in the conditions of conjugate natural convection. *J Eng Therm Phys* 2010;19:119–27.
- [17] Kuznetsov GV, Sheremet MA. A numerical simulation of double-diffusive conjugate natural convection in an enclosure. *Int J Therm Sci* 2011;50:1878–86.
- [18] Sun H, Lauriat G, Sun DL, Tao WQ. Transient double-diffusive convection in an enclosure with large density variations. *Int J Heat Mass Transfer* 2010;53:615–25.